ChemPubSoc Europe
DOI: 10.1002/cctc.201402857
CHEMCATCHEM
Full Papers

Investigation of Ce–Zr Oxide-Supported Ni Catalysts in the Steam Reforming of *meta*-Cresol as a Model Component for Bio-Derived Tar

Thi Minh Chau Hoang, N. Koteswara Rao, Leon Lefferts, and K. Seshan*[a]

Phenols are major components in the tar vapours formed during gasification of biomass-based feedstocks. The steam reforming of *m*-cresol was demonstrated for tar removal and H_2 production in this study. Ceria–zirconia based catalysts containing nickel were developed and investigated by using multiple characterisation techniques such as X-ray diffraction, Raman spectroscopy, X-ray photoelectron spectroscopy, and temperature-programmed reduction and oxidation. These catalysts show high activity and excellent stability for producing hydrogen. The influence of the preparation method for the support on the catalyst performance was studied. Ni deposited on a hydrothermally prepared Ce–Zr solid solution was shown to be the most promising catalyst because of its excellent anti-coking properties resulting from its high oxygen mobility. Insight into the steam-reforming reactions was gained by in situ FTIR spectroscopy. The IR results reveal different geometries of adsorbed *m*-cresol on the different supports. It also indicates that multiple sites (Ni and Ce) on the catalysts are involved in the reactions.

Introduction

With the depletion of fossil fuels, efforts in developing a technology for conversion of alternative sources for energy and chemicals have been intensified, especially focusing on the aspect of sustainability. Biomass, tide, solar energy and wind are considered as sustainable resources for fuels and energy. Among them, biomass is the only renewable resource that contains carbon. Transportation fuels or fuel precursors can be produced from biomass by direct approaches (e.g., pyrolysis for bio-oil, dehydration of carbohydrates to 5-hydroxymethylfurfural etc.) or indirectly by gasification for synthesis gas production followed by Fischer–Tropsch conversion.[1] As bio-oil and bio-derived platform chemicals have high O contents,[1] deoxygenation upgrading of these components is mandatory to meet the requirement for fuels. Hydrogen is a key component for upgrading bio-oil through hydro-deoxygenation, and for hydrogenation of platform chemicals from biomass, e.g., sorbitol from cellulose. Demand for hydrogen is omnipresent in the biorefinery.[2] Minimisation of the use of H_2 from external sources, especially from fossil resources is obligatory for the production of bio-fuels.[2] Hydrogen can be obtained from biomass-based feedstocks by gasification, e.g., steam reforming or partial oxidation.[1,3–5] As biomass is unstable under the elevated temperatures required for gasification, devolatilisation and formation of tars occur.[4,6] Tar gasification is, thus, an important issue from the point of view of complete utilisation. Removal of tar is also essential for making high-purity H_2 for subsequent processes or its use in fuel cells. Phenols and phenolic components such as cresols account for the largest fraction in the composition of tars derived from bio-feedstocks.[1,7] In our previous paper[8] on steam reforming of humin-based by-products, we also addressed the issue of cresols and phenol as the major volatile components, which were formed during the heating of humin to the gasification temperatures. For studying steam reforming of tars, model components such as phenol, benzene, toluene or acid acetic are normally chosen. The number of research studies involving steam reforming of cresols is very limited.[9–12] *m*-Cresol is a good probe molecule for study in the steam reforming of biomass because of its multiple chemical functionalities, namely aromatic ring, hydroxyl and alkyl substitutions. These chemical groups are widely present in most bio-derived tars.[13] Certainly, cresols are typical degradation components of cellulose-derived humin waste. In this study, *m*-cresol is selected as a model component for the development of a catalyst for the steam reforming of volatiles formed during gasification of humins, and in general for the gasification of bio-oil and tars for hydrogen production.

Commercial steam-reforming nickel catalysts have been widely used for tars gasification.[6,13] Ni catalysts display high, demonstrated activity.[6] However, the disadvantage of Ni catalyst in reforming of tars is the rapid deactivation, mainly as a result of coke formation. For example, coke deposition rate in steam reforming of *m*-cresol was as high as 20–140 mg coke $g_{catalyst}^{-1}h^{-1}$ if a Ni/MgO commercial catalyst (WC series supplied by Wuxi Qiangya Co., Ltd.) was used.[9] Ishihara

---

[a] *Dr. T. M. C. Hoang, N. K. Rao, Prof. Dr. L. Lefferts, Prof. Dr. K. Seshan
Catalytic Processes and Materials
Faculty of Science & Technology, MESA+ Institute for Nanotechnology
University of Twente
7500 AE Enschede, The Netherlands
E-mail: k.seshan@utwente.nl
Homepage: www.utwente.nl/tnw/cpm*

Supporting information for this article is available on the WWW under http://dx.doi.org/10.1002/cctc.201402857.

et al.[11] reported that both conversion of *m*-cresol and hydrogen yield dropped from 100 to approximately 80% within 4 h if the 15 wt% Ni–2 wt% Ru/MgO–La_2O_3–Al_2O_3 catalyst was used. Tomisghe's group designed an effective catalyst, Ni/CeO_2–Al_2O_3 for removal of tars from biomass by auto-thermal reforming, i.e., in the presence of oxygen.[14] They claimed that the "excellent performance"[14] of the catalyst was a result of the strong interaction of Ni with CeO_2, and explained this as caused by the oxygen mobility between Ni and CeO_2.

In general, CeO_2 is a key component of commercial catalysts if oxidation is required such as in three-way automotive exhaust gas clean-up systems.[15] It has facile redox properties and oxygen storage capacity, which facilitate oxidation reactions. As gasification is essentially an oxidation reaction with H_2O or CO_2, the use of CeO_2 as a support or promoter for steam-reforming catalysts may also improve the oxidation of coke. Oxygen mobility of CeO_2 is much enhanced by introducing foreign ions such as Zr^{4+}, Gd^{3+} or Tb^{4+} into the CeO_2 lattice.[16,17] According to Di Monte et al.,[16,18] the oxygen ion mobility within the crystal lattice originated from the formation of a defective solid solution in which, for example, Zr^{4+} (ionic radius 0.84 Å) replaces some Ce^{4+} cations (ionic radius 0.96 Å). Previous work in our group on the steam reforming of phenol demonstrated that Ni/CeO_2–ZrO_2 catalyst, in which CeO_2 was impregnated on ZrO_2 oxide prior to the deposition of Ni, was an active and stable catalyst.[19] In this study, the influence of ceria–zirconia mixed oxide supports on Ni based catalysts for the steam reforming for the *m*-cresol is investigated.

Results and Discussion

Catalyst characterisation

Ceria–zirconia-based supports were prepared by co-precipitation, co-precipitation followed by hydrothermal treatment and impregnation techniques and denoted CP, HT and IM, respectively (see the Experimental Section for details). The catalysts with Ni deposited are named as Ni/CP, Ni/HT and Ni/IM, respectively.

In Figure 1, the XRD spectra of the prepared supports are shown. The XRD pattern of the IM support inherits all the major structural features of its initial support precursor, i.e., *m*-ZrO_2. However, the main peak at approximately 28° shifts to 28.2° with an asymmetric shape. This shift might be the result of the overlapped peak of cubic CeO_2 (111), which appears at 28.55°. In addition, two distinct peaks of CeO_2 were found at 33.1 and 47.4°, which correspond to CeO_2 (200) and CeO_2 (220), respectively. Thus, the IM support is a mixture of CeO_2 and ZrO_2 oxides. In contrast, the CP support contains only one single tetragonal phase of ZrO_2, which indicates that CeO_2 distributes homogenously in the ZrO_2 lattice to form a solid solution. The XRD spectrum of HT support indicates the presence of both tetragonal and monoclinic phases without any segregation of CeO_2. The transition of tetragonal to monoclinic has also been claimed to be caused by the influence of the strong alkaline medium (i.e., 40 wt.% KOH) used in the hydrothermal step.[20]

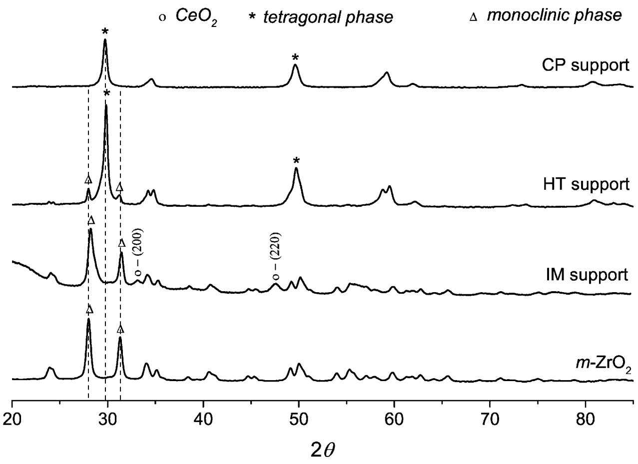

Figure 1. XRD spectra of catalyst supports.

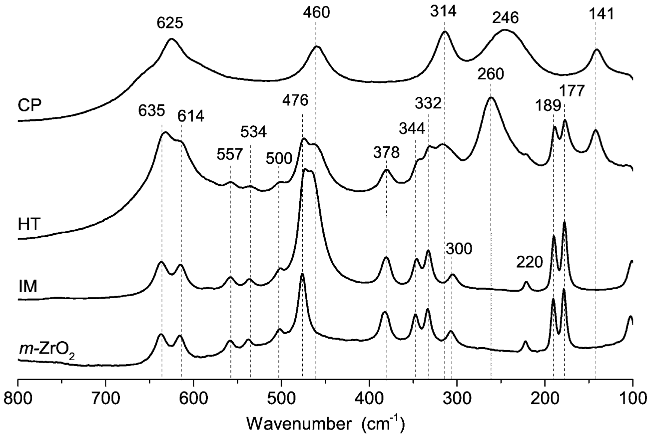

Figure 2. Raman spectra of catalyst supports.

The Raman spectra of CeO_2–ZrO_2 supports are presented in Figure 2. The assignment of vibration frequencies was based on the work by Kim and Hamaguchi,[21] Anastassakis et al.,[22] Hirata et al.,[23] Hirata[24] and Kim et al.[25] and summarised in Table S1 (Supporting Information). As a reference, Raman spectra of *m*-ZrO_2 (calcined at 800 °C, 6 h) were recorded in which 14 (of the 18) observed active modes of monoclinic structure were in agreement with those in the others' work. The IM support exhibited all these frequencies, besides a broad peak in the region of approximately 470 cm^{-1}. This broad band is attributed to overlapping of the peak at approximately 476 cm^{-1} (A_g mode of ZrO_2) and the peak at approximately 465 cm^{-1} (F_{2g} of CeO_2).

On the other hand, for CP support, the observed six frequencies ($1\,A_{1g}+3\,E_g+2\,B_{1g}$) are typical for a tetragonal structure. The Raman spectrum of HT support shows features indicating the presence of both monoclinic and tetragonal phases. The Raman spectral results are thus in excellent agreement with the XRD results. The shift to the higher value of the E_g mode at 246 cm^{-1} in the case of HT support was attributed to the decrease in the lattice parameter because of the solid solution formation resulting in a lower metal–oxygen bond length.[18]

The physicochemical characteristics of the catalysts are summarised in Table 1. Catalysts made with the IM and HT supports

Table 1. Physical and chemical properties of the catalysts.

Sample ID	BET specific area	V_{pore}	Bulk elemental composition based on XRF			Surface composition based on XPS		
	$[m^2 g^{-1}]$	$[cm^3 g^{-1}]$	Ni/Ce/Zr (atomic ratio)	Ce/Zr (atomic ratio)	Ni [wt%]	Ni/Ce/Zr (atomic ratio)	Ce/Zr (atomic ratio)	Ni (count)
CP	10	0.11	n.a.	n.a.	n.a.	n.a.	n.a.	n.a.
HT	53.7	0.3	n.a.	n.a.	n.a.	n.a.	n.a.	n.a.
Ni/CP[a,c]	2.7	0.01	3/10.8/85.2	0.12	1.7	8.3/12/79.7	0.15	44952
Ni/HT[b,c]	42.2	0.29	7.1/15.3/76.8	0.2	3.2	14.7/16.1/69.2	0.23	48515
Ni/IM[d]	35.4	0.47	6/16/78	0.2	2.9	18.7/27.4/53.9	0.51	55645

[a] Ni/CP catalyst contains ≈1.5 wt% HfO_2 and [b] Ni/HT catalyst contains ≈1.34 wt% HfO_2 (based on XRF result); [c] these catalysts also contain a trace amount of K (≈0.06 wt%), which probably came from the ammonia solution used in co-precipitation step; [d] Ni/IM contains a trace amount of Fe (≈0.04 wt%). K or Fe was not detected by XPS.

have higher surface areas and pore volume even after severe heat treatments (725 °C calcination and 650 °C reduction). In comparison, CP-based catalysts exhibit low surface areas. In general, the texture of the Ce–Zr–O solid solution strongly depends upon synthesis parameters such as type of precursors, precipitation agent (OH^- source), time, calcination temperature etc. The BET specific area of CP support of 10 $m^2 g^{-1}$ is lower than that of the Ce–Zr solid solution for similar Ce/Zr ratios reported in the literature.[17,26–27] However, the authors of those works used slightly different preparation recipes. For example, Hu et al.[27] used $ZrOCl_2$ and $Ce(NO_3)_3{\cdot}6H_2O$ as precursors, and the support was calcined at only 600 °C for 6 h. Consequently, the obtained $Ce_{0.1}Zr_{0.9}O_2$ oxide had a specific area of 42.97 $m^2 g^{-1}$. Biswas and Kunzru[26] also used similar synthesis conditions with a higher calcination temperature (750 °C) and they obtained a mixed oxide $Ce_{0.16}Zr_{0.84}O_2$ with a specific area of 31.1 $m^2 g^{-1}$. Colón et al.[17] used nitrate precursors, however, the mixed oxide was calcined under H_2O-enriched gas. Therefore, the low specific area of CP in our case can be caused by the experimental synthesis parameters that were used. However, by introducing the subsequent hydrothermal step, the specific area (HT) was much improved, from 10 to 53.7 $m^2 g^{-1}$. This improvement might be the result of the conversion of the hydroxide complex to the oxide form (the hydroxide complex is formed in the co-precipitation step). Thus, it possibly inhibits the grain growth and fusion of the as-prepared hydrated mixed hydroxide during the calcination step at high temperature.[28] Furthermore, Ni metal deposition with subsequent thermal treatment steps (e.g., calcination and reduction) influenced the texture of the catalyst. For example, after deposition of Ni or Rh on CeO_2–ZrO_2-based supports, loss of 20–33 % specific area was reported elsewhere.[26–27,29] In this study, the CP support also experienced severe sintering during deposition and post-treatment of Ni-supported catalyst. Its specific area reduced by approximately 80 % and the pore structure almost collapsed. In contrast, HT-based catalyst lost only approximately 21 % of its original specific area. Therefore, the hydrothermal treatment improves not only the texture of the as-prepared support, but also the thermal resistance of the corresponding catalyst.

In Table 1, the elemental compositions of the catalysts, the bulk (based on X-ray fluorescence analysis, XRF) and the surface (based on X-ray photoelectron spectroscopy, XPS) are also shown. As the depth of information in XPS technique is below 3 nm, it is reasonable to consider that the data obtained from XPS are representative for the surface composition. The surface atomic Ce/Zr ratios, respectively, for Ni/HT and Ni/CP are very close to the corresponding ratios in the bulk phase as estimated from XRF analysis. This confirms an even distribution of ceria in the ceria–zirconia solid solution formed in these two cases. The slightly enriched ceria content on the surface is attributable to migration of Ce^{4+} during reductive treatment.[30] In contrast, the surface Ce/Zr atomic ratio of Ni/IM catalyst is much higher than in the bulk (0.51 compared with 0.2). This result is expected as ceria was deposited through impregnation on ZrO_2 oxide. The atomic concentration of cerium on the surface is highest in the case of Ni/IM catalyst. XRF analysis revealed trace amounts of potassium in both Ni/CP and Ni/HT catalyst, which came from the co-precipitation step. However, no potassium was detected by XPS, which indicates its absence on the surface of the catalyst. Thus, this trace amount of potassium is not expected to have any contribution to the differences in activity of the catalysts.

From Table 1, it is realised that the weight percentage of Ni on Ni/IM is approximately 10 % lower than that on Ni/HT (2.9 vs. 3.2 wt%). On the other hand, the absolute counts for Ni band in the XPS spectra of Ni/IM and Ni/HT are 55645 and 48515, respectively. These values are proportional to the Ni content per catalyst surface area. If the specific areas of each catalyst are accounted (Ni/IM 35.4 $m^2 g^{-1}$ and Ni/HT 42.2 $m^2 g^{-1}$), the specific surface areas of Ni particles are similar for both Ni/IM and Ni/HT. On the other hand, for Ni/CP both surface and bulk amounts of Ni are much lower than for the other catalysts. Consequently, this can be expected to have a large influence on the activity of the catalyst. TEM analysis and hydrogen chemisorption were employed to measure the Ni dispersion. However, owing to the low contrast between Ni and the support (Ce and Zr have higher molecular mass than Ni) and the spill-over phenomenon of H_2 on ceria, these techniques were not suitable. Qualitatively, comparison of Ni surface area on those catalysts could only be relied on XPS data.

In addition, XPS can also help to understand the surface chemical state of cerium in the catalysts. In Figure 3 the XPS Ce $3d_{5/2}$ core–level spectra of the catalysts and corresponding deconvolution curves are shown. The experimental photoemission band of Ce $3d_{5/2}$ was deconvoluted into three peaks

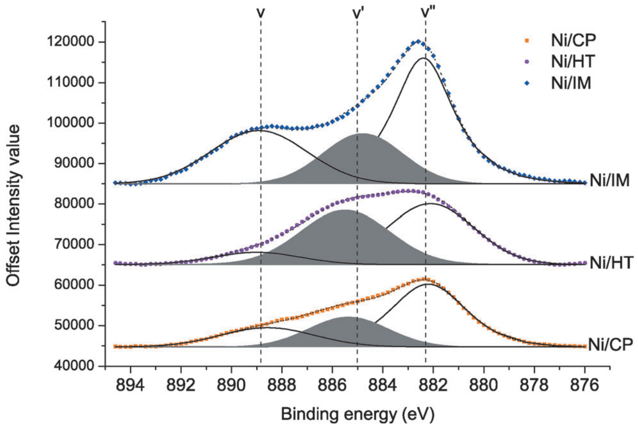

Figure 3. XPS Ce 3d$_{5/2}$ spectra of supported Ni catalysts and deconvolution. Area curve filled with grey is representative for Ce^{3+} content.

and denoted as: v (882.25 ± 0.0.15 eV), v′ (885.15 ± 0.35 eV) and v" (888.7 ± 0.2 eV) according to Laachir et al.[31] and Pfau and Schierbaum.[32] X-ray satellites and the Shirley background were subtracted prior to deconvolution. v and v″ were assigned to mixing of the $3d^94f^2V^{n-2}$ and $3d^94f^1V^{n-1}$ Ce^{4+} state. v′ was attributed to $3d^94f^1V^n$ Ce^{3+} state. These assignments are in accordance with the reported literature.[31–33] Quantitative determination of Ce^{3+} concentrations is calculated from area percentage of the v′ band and summarised in Table S2. The data in Table 1 as well as those in Figure 3 indicate that Ce^{3+} concentration/amount is the highest in Ni/HT among the three catalysts. It should be remarked that there is a high chance that the sample surface is re-oxidised owing to exposure to ambient condition when the catalysts were transferred from reactor to container vials as well as during compressing on Ir foil for XPS measurement. Therefore, the oxidation state of Ce is investigated further by using temperature programmed reduction (TPR) analysis.

The TPR profiles of the catalysts and the corresponding supports are shown in Figure 4. The H$_2$ uptakes and other related details are given in Table 2. The TPR curve of IM support shows only a small peak at approximately 650 °C. The H$_2$ uptake during reduction of the IM support was much lower (see Table 2) than that required for full/bulk reduction of Ce^{4+} to Ce^{3+}. It is reported that bulk Ce^{4+} is reduced only at elevated temperatures, above 850 °C.[29,34] However, another reduction peak in the range of 450 to 750 °C is reported for pure ceria, depending on the size and morphology of the ceria particles. This is often attributed to reduction of Ce^{4+} at the surface.[26,34] Therefore, the low H$_2$ uptake in the reduction of IM support (at 650 °C) indicates the presence of ceria as a separate phase and the reduction peak corresponds to Ce^{4+}, probably present at the external surface of Ce particles or Ce in the vicinity of ZrO$_2$. CP and HT support exhibit a major peak at approximately 700 °C and 500 °C, respectively, whereby it was shown earlier that ceria is distributed well in the zirconia phase forming solid solutions. The reduction temperatures of these oxide solutions are in the same temperature range as those reported for ceria–zirconia solid solutions with similar Ce/Zr ratios.[16,35] The lower reduction temperature of HT support than that of CP support can be attributed to an increase of the cerium content in the support.[16,34] The percentage of Ce^{3+} in CP support was higher than that in HT support: 91 % compared to 79 %, respectively (Table 2). This high Ce^{3+} content indicates that the reduction also takes place in the bulk phase of the mixed oxides.

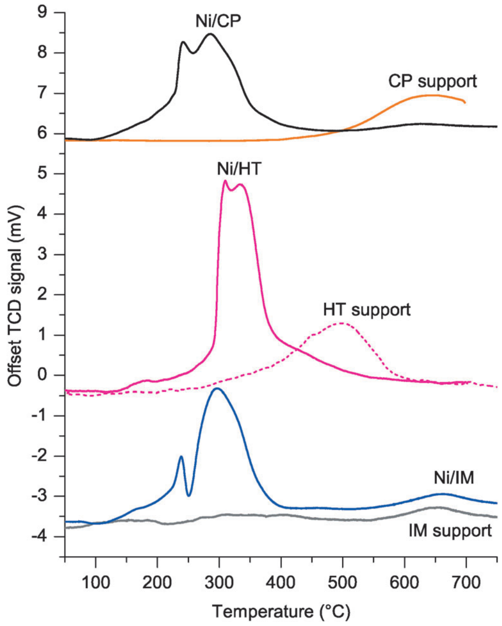

Figure 4. TPR curves of ceria–zirconia-based supports and the corresponding catalysts with supported Ni. Reduction flow rate 5 vol. % H$_2$/Ar (25 cm^3 min^{-1}), temperature ramp 5 °C min^{-1}.

The TPR patterns of the catalysts containing Ni are different from those of the corresponding supports. In all cases, two reduction peaks are observed, differing in intensities as well as temperature. These reduction peaks appear below 400 °C. Reduction is initiated at relatively lower temperatures (125–150 °C) and the reduction peaks are broad, whereas uptake of H$_2$ at low temperature is not seen in reduction of bare supports. These two phenomena are often ascribed to an interaction between the transition metal (i.e., Ni in this case) and the

Table 2. Hydrogen consumption during TPR analysis.

Sample ID	TPR H$_2$ uptake [mmol g^{-1}]	Theoretical H$_2$ uptake [mmol g^{-1}] Ce^{4+}→Ce^{3+} (U_{Ce})	Ni^{2+}→Ni^0 (U_{Ni})	Ce^{3+} content[a] [%]
CP	0.39	0.43		91
HT	0.49	0.62		79 ± 3.2
IM	0.05	0.646		7.8
Ni/CP	0.65	0.42	0.23	100
Ni/HT	1.02 ± 0.04	0.59	0.55	80 ± 6.7
Ni/IM	0.83 ± 0.1	0.62	0.47	58 ± 16

[a] Ce^{3+} (%) = 100 % × (U_{TPR} − U_{Ni})/U_{Ce}, in which U_{TPR}, U_{Ce}, and U_{Ni} represent H$_2$ uptake in the TPR experiment and the theoretical H$_2$ uptake for reduction of Ni^{2+} (to Ni^0) and Ce^{4+} (to Ce^{3+}), respectively. We assume that, besides the reduction of Ni, H$_2$ uptake is only consumed for the following reaction: $2CeO_2 + H_2 \rightarrow Ce_2O_3 + H_2O$.

ceria-based support.[36] Reducibility of Ni is facilitated if supported on CeO_2 or Ce–Zr oxide.[14,36] The uptake of H_2 at a relatively low temperature (onset at 125 °C) is attributed to the spillover of H_2 on the support.[37–38] This phenomenon requires the presence of a metal to activate H_2.[37] Furthermore, the interaction between Ni and CeO_2 may help reduce the Ce^{4+} species not only on the surface but also the species located inside the lattice. The reduction of ceria by H_2 in general can be associated with the oxygen storage capacity of the catalyst support. According to the estimation of H_2 uptake from Table 2, Ni/HT catalyst potentially has the highest oxygen vacancies among the three catalysts, owing to the amounts of reducible Ce^{4+}, thus maximising the redox capacity of the catalyst.

Catalytic tests

Among the three catalysts, Ni/CP has the lowest Ni content, low surface area, and correspondingly exhibited a low catalytic activity. It also deactivated severely, losing >60% of its activity during 8 h time-on-stream. In Figure 5, the results of steam reforming of *m*-cresol using Ni/HT and Ni/IM catalysts during 30 h TOS are shown. The products identified for *m*-cresol reforming were phenol, benzene, toluene, CO, CO_2 and hydrogen. Carbon balance of 100±3% was achieved during all the kinetic experiments. Both catalysts gave a very high initial conversion of *m*-cresol, 98% and 95% for Ni/HT and Ni/IM, respectively (Figure 5 A). The main products were CO, CO_2, H_2 and trace amounts of phenol (yield below 0.1%). The initial selectivities (Figure 5 B) towards CO_2 and CO for both catalysts were similar: for CO_2 approximately 85% and for CO approximately 15% in carbon balance, which is lower than the equilibrium selectivity estimated at this condition (for CO_2 ≈96.5% and CO ≈3.5%). The corresponding initial hydrogen yields were 89% and 87% when using Ni/HT and Ni/IM, respectively. The conversion of *m*-cresol gradually decreased (Figure 5 A) in both cases over 25 h TOS and then the conversion started stabilising, showing partial deactivation (no change in conversion was observed after 27 h TOS). The drop in conversion for Ni/IM catalyst was higher than that for Ni/HT catalyst (Ni/HT from 99% to 80%; Ni/IM from 95% to 63% after 30 h TOS). There was also a corresponding decrease in yields of gaseous products. Surprisingly, the product selectivity to CO_2 and CO, in the case of Ni/HT, remained almost constant. In contrast, for Ni/IM catalyst, these selectivities varied with time: CO increased from 14.9% to 29.7% and CO_2 decreased from 85.1% to 69.1% after 30 h TOS. This implies that the water gas shift activity of Ni/HT is more stable than that of Ni/IM catalyst. Owing to the lower extent of overall deactivation and better water gas shift stability, H_2 yields for Ni/HT decreased less appreciably than for Ni/IM. Thus, among the three catalysts, Ni/HT is the most promising one. This study has proved that hydrothermal ceria–zirconia oxide is effective and has high potential as a catalyst support in steam reforming of *m*-cresol and presumably also of tars. Therefore, optimisation of the support synthesis (hydrothermal temperature, retention, Ce/Zr ratio) is required. This matter will be subjected to further studies.

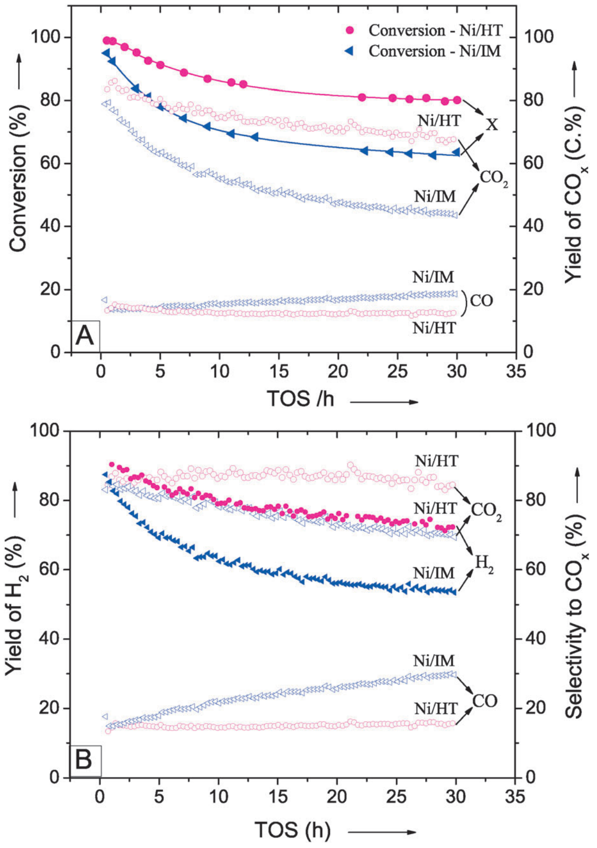

Figure 5. Catalytic steam reforming of *m*-cresol using Ni/HT and Ni/IM catalysts with the reaction condition: 700 °C, S/C≈43:1, $WHSV_{m\text{-cresol}}$ 7.89 h^{-1}. A) Conversion of *m*-cresol and yield of CO_x. B) Yield of H_2 and selectivity to CO_x. TOS = Time-on-stream.

The identified products in steam reforming of *m*-cresol using bare HT support are illustrated in Figure 6. The HT support already exhibits some initial activity for the decomposition/reforming of *m*-cresol. This activity decreases rapidly within the first hour then reaches steady state after 2 h TOS. For example, the phenol yield dropped from 0.5% at 0.5 h to 0.15% and continued at this level. Similar observation can also be made in the case of CO and CO_2. Benzene and toluene were not observed in these experiments. These results imply activation of *m*-cresol on the support. It should be noted that the yields of phenol, benzene, toluene or CO_x were negligible (e.g., phenol 0.03–0.08%) for thermal steam reforming (in the absence of a catalyst). Therefore, the yields of CO_x, if the reaction reaches steady state (i.e., after 2 h TOS), are attributed to a combination of the residual activity of the support and the coke deposits on the support.

Characterisation of coke deposits on used catalysts

The nature of the coke deposited on used catalysts was investigated by Raman spectroscopy. In Figure 7 the primary order Raman spectra of coke normalized to the band at 1595 cm^{-1} (G band) are shown. It can be seen that Raman spectra of coke deposited on supports contain two broad and strongly overlapping peaks, at approximately 1350 cm^{-1} (D band) and at

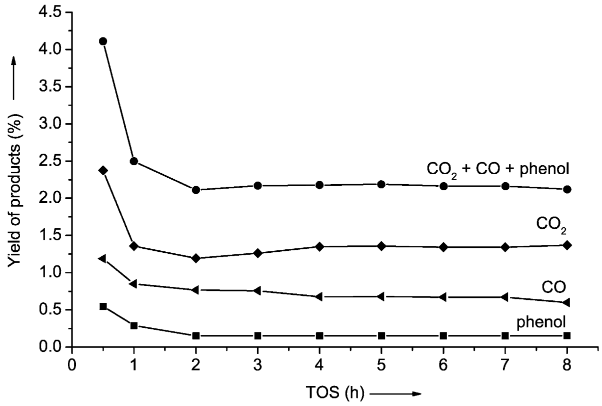

Figure 6. Product yields from steam reforming of *m*-cresol on bare HT support. Reaction condition: 700 °C, S/C ≈ 43:1, WHSV 7.89 h^{-1}.

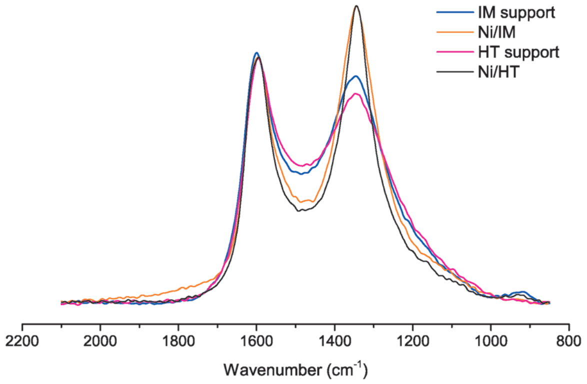

Figure 7. Raman spectra of coke deposited on the catalysts, normalised to G band at 1595 cm^{-1}.

1595 cm^{-1}. With regard to the relatively low oxidation temperature of these cokes (310–321 °C, from temperature programmed oxidation, TPO, Figure 8), these two bands cannot be assigned to graphitic crystallite structures or disordered graphite. The G band here can be attributed to the aromatic ring breathing[39] or the bond stretching of all pairs of sp^2 carbon atoms[40] (in both rings and chains). The D band corresponds to the breathing mode of sp^2 C in (poly)aromatic rings.[39–41] The Raman spectra of coke deposited on both Ni-supported catalysts (Ni/HT and Ni/IM) exhibit similar shapes. Compared with the Raman spectra of coke deposited on bare support, both D and G bands of the Raman spectra of coke on supported Ni catalysts are sharper with narrower line width. It is also apparent that D band to G band intensity ratios (I_D/I_G) of the coke on Ni catalysts are higher than those of bare supports. The differences in the Raman spectra, together with the slightly higher oxidation temperature, indicate an increase in the order of the carbon-based structure in the case of supported Ni catalysts. This also implies a lower hydrogen content and increase of ring concentration in coke deposited on supported Ni catalysts compared with coke on bare support. Coke formed during steam reforming of *m*-cresol using bare supports might be caused by decomposition/condensation of *m*-cresol, resulting in probably polyaromatic carbon species. As Ni is capable of disassociating C–C or C–H bonds of *m*-cresol, the coke formed in the presence of Ni catalyst might be the result of recombination of intermediates formed on the metal surface. Therefore, more graphitised coke is expected.

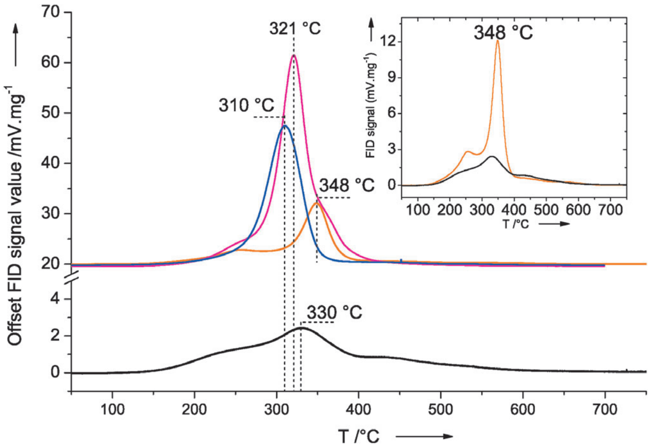

Figure 8. TPO of coke deposits on the supports only and catalysts: IM (—); HT (—); Ni/IM (—); Ni/HT (—). Inset: coke on Ni/HT (—) and Ni/IM (—) in comparison. Condition: 1 vol.% O_2/Ar, 75 $cm^3\,min^{-1}$, split ratio to methaniser ≈ 5/75, temperature ramp 5 °C min^{-1}.

The quantification of coke deposited on the catalysts during steam reforming of *m*-cresol was achieved by TPO, which is illustrated Figure 8. In the case of the supports only, the amount of coke was higher for HT than for IM support (C 4.2 wt% vs. C 2.9 wt%). This implies that the adsorption amount of *m*-cresol is more enhanced on HT than on IM. This will be discussed in the next section on probing the reforming steps by in situ FTIR spectroscopy. Nevertheless, coke formation on supported Ni catalysts was lower and showed the opposite trend. The amount of carbon deposited on Ni/HT (0.79 wt%) was half of that on Ni/IM (1.58 wt%). Albeit its higher surface cerium content, the latter catalyst (Ni/IM) contains a lower amount of Ce^{3+} (according to TPR result). Under steam reforming conditions, the support can be re-oxidised by H_2O or CO_2. Thus, higher reducible oxygen capacity can be achieved with Ni/HT catalyst. In addition, HT exhibits the lowest reduction temperature among the supports, which correlates to more facile removal of oxygen on the support lattice. Together, the higher amount of labile oxygen can enhance the oxidation of the coke or the carbon amounts deposited on the catalyst under reforming condition. Therefore, it can explain the lower coke content on used Ni/HT catalyst. The presence of coke on supported Ni catalysts is one of the causes of deactivation of the catalysts. In agreement to this, Ni/HT catalyst showed the lowest extent of deactivation, and most promise for steam reforming of *m*-cresol. On the other hand, other possible reasons for catalyst deactivation such as reduction of specific area or metal sintering could not be characterised because of the low amounts of used catalyst and poor statistical results from TEM (explained above in the catalyst-characterisation section).

In situ FTIR of steam reforming of *m*-cresol on HT- and IM-based catalysts

FTIR spectroscopy was employed to investigate the interaction of *m*-cresol with catalyst and the subsequent steam reforming steps. To observe the interaction of the reactants with the support, a titration-type reforming experiment was performed in a FTIR cell. Owing to the strong IR absorption at high temperature, resulting in loss of IR signal, FTIR measurements could only be conducted at more moderate temperatures. The self-supporting discs of the catalysts were first reduced in 10 vol.% H_2/He at 450 °C for an hour and then the IR cell was flushed with He. For the reforming steps, catalyst discs were exposed to He flow containing each reactant (first *m*-cresol then H_2O) for 1 h; the two steps were separated by an evacuation step for 30 min in He to remove weakly or physically adsorbed species. In Figure 9 A and B, the IR spectra recorded at the end of each step are shown. Prior to adsorption of *m*-cresol, both IM and HT supports exhibit two sets of peaks: (i) O–H stretching, ν_{OH} (3800–3200 cm^{-1}) and (ii) C–O stretching (ν_{CO}) in carbonate or carboxylate between 1600 and 1300 cm^{-1}.[42] In the ν_{OH} range, the spectra of both supports show a strong peak at 3664 cm^{-1}, which can be assigned to tri-bridging hydroxyls and a broad band in the range of 3500–3300 cm^{-1}, which corresponds to hydrogen-bridging hydroxyls. In addition, in the case of IM support, the main peak at 3664 cm^{-1} has a small shoulder at approximately 3745 cm^{-1}, which is attributed to low-coordinated hydroxyl of *m*-ZrO_2.[43] For the HT support, the spectral ν_{OH} range consists of a weak peak at 3721 cm^{-1}, which may be tentatively assigned to bi-bridging OH.[44] The IR spectrum of reduced *m*-ZrO_2 does not exhibit any clear peaks in the ν_{CO} range (not shown here). This is in agreement with the results on reduced ZrO_2 reported elsewhere.[45] Therefore, the presence of ν_{CO} in the IR spectra of both supports indicates the ceria fraction of the support. The peak in the ν_{CO} band of IM support centres at 1450–1375 cm^{-1}, a range that mainly represents polydentate carbonate stretching (1462 cm^{-1}, 1351 cm^{-1}).[46] On the other hand, the ν_{CO} band of HT support spreads over the range of 1600–1400 cm^{-1}, which comprises bands of bi-dentate (1567 cm^{-1}), mono-dentate (1504 cm^{-1}) and bi-carbonate (1414 cm^{-1}).

The spectra of support after adsorption of *m*-cresol vapour as well as the subsequent exposure to steam consist of three distinct sets of peaks: (i) O–H stretching vibration (ν_{OH}) between 3750 and 3200 cm^{-1}, (ii) C–H stretching vibration (ν_{CH}) between 3100 and 2800 cm^{-1} and (iii) the set between 1600 and 1000 cm^{-1}. The last set contains a complex combination of multiple vibrations including skeletal aromatic ring stretching, C–O stretching (ν_{CO}), alkyl deformation etc. Discussing in detail what occurs during each reaction step is beyond the scope of this paper. However, the apparent differences in relative intensities of the main peaks (e.g., ν_{CH} vs. peak at ≈1570 cm^{-1} or peak at 1475 cm^{-1}) implies different reaction pathways occurring on these supports. The assignments for the main peaks of IR spectra is summarised in Table 3.

The spectra recorded after outgassing the *m*-cresol adsorbed on the support surface represent the chemisorbed *m*-cresol or intermediates on the supports. It is clearly observed that the $\nu_{C-H)}/\phi$ (peak at 3052 cm^{-1} vs. peak at 1575 cm^{-1}, respectively) intensity ratio of IM is much lower than that of HT. This can indicate the orientation of adsorbed molecules on the surface. If the aromatic rings are adsorbed horizontally (in parallel direction on the surface), the H can interact with OH or carbonate groups on the support surface through hydrogen bonds. This would hinder the C–H stretching vibrations (3052 cm^{-1}), thus leading to lower ν_{C-H}/ϕ ratio. In contrast, if *m*-cresol is adsorbed perpendicularly on the support through the phenol group or methylene group, hydrogen bonding between the groups on the support surface and H of the ring is minimised. A comparison of the IR spectra of *m*-cresol adsorbed on the two supports and the attenuated total reflectance IR spectrum of free liquid *m*-cresol in the low wavenumber range is shown in Figure 10 (all the spectra were normalised to the intensity of the band at ≈1600 cm^{-1}). It can be seen that the spectral pattern of HT resembles more closely that of free *m*-cresol. In addition, the band at approximately 1350 cm^{-1} of free *m*-

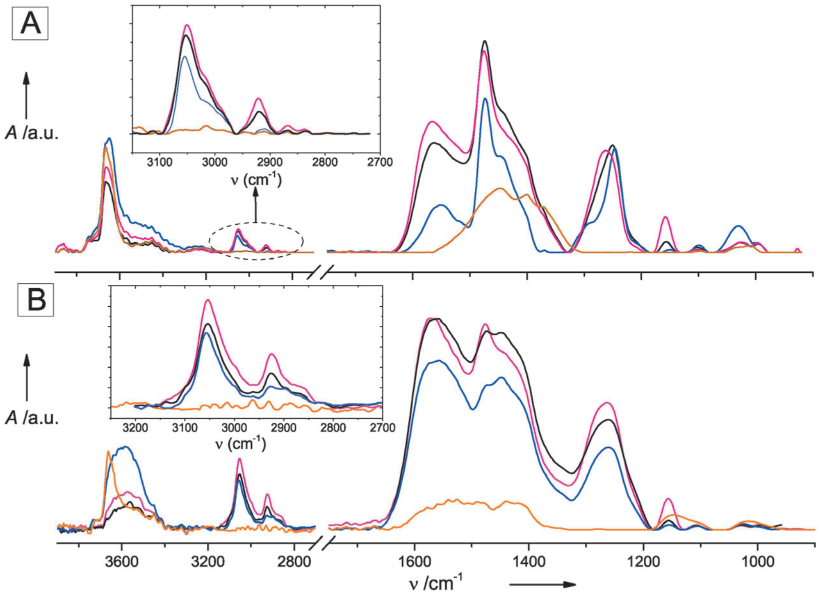

Figure 9. FTIR spectra recorded under titration-typed steam reforming of *m*-cresol on A) IM support and B) HT support. He after reducing in H_2/He (——); adsorption of 128 ppm *m*-cresol/He (——); He after adsorption of *m*-cresol/He (——); adsorption of He saturated with steam (——). Conditions: 450 °C, exposure to He flow of 20 $cm^3 min^{-1}$ containing reactant (128 ppm *m*-cresol or saturated H_2O at 21 °C) for 1 h, outgassed in He for 30 min. Insets: Enlargement of the C–H stretching vibration (ν_{CH}) region between 3100 and 2800 cm^{-1}.

Table 3. Assignment of peaks in FTIR spectra recorded in steam reforming of *m*-cresol on Ce–Zr supports.[a]

IM	HT	Assignment
3745 (w)		terminal O—H stretching (ν_{OH})
3721 (w)	3721 (w)	bi-bridged O—H stretching (ν_{OH})
3645 (s)	3645 (s)	tri-bridge O—H stretching (ν_{OH})
3300–3500 (b)	3300–3500 (b)	hydrogen-bonded OH
3050 (m)	3052 (m)	C—H stretching of aromatic ring (ν_{CH})
2921 (w)	2925 (mw)	asymmetric C—H stretching of CH_2/CH_3 (ν_{CH}/ν_{CH_3})
2867 (vw)	2860 (sh)	symmetric C—H stretching of CH_2/CH_3 (ν_{CH2}/ν_{CH3})
1540–1565 (s)	1556–1575 (s)	quadrant stretching of the ring (ϕ)
1471–1473 (vs)	1473–1477 (s)	ring deformation ($\delta_{ringC=C}$)
1440–1446 (sh)	1446 (s)	alkyl deformation (δ_{CH_3} or δ_{CH_2})
	1362 (sh)	OH deformation (δ_{OH})
1240–1290 (s)	1260–1280 (vs)	C—O stretching (ν_{C-O})

[a] w: weak, s: strong, b: broad, m: medium, vw: very weak, vs: very strong, sh: on shoulder.

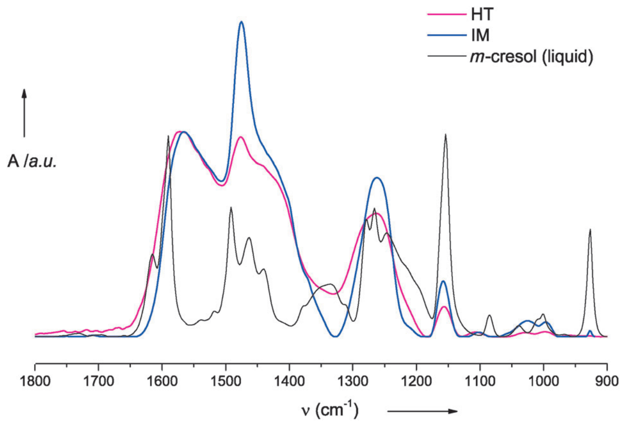

Figure 10. Comparison of adsorbed *m*-cresol on IM and HT support with pure *m*-cresol at 21 °C. The IR spectra are normalised to the peak at ≈1590 cm^{-1}. Conditions: FTIR at 450 °C for HT and IM; attenuated total reflectance IR at room temperature for *m*-cresol.

cresol, which is assigned to deformation vibration of OH group (δ_{OH}), is absent in the spectrum of IM but it is present in the spectrum for HT. This implies that deprotonation of OH takes place on IM support to form an adsorbed phenolate and in the case of HT support the phenolic group remains intact. Increasing electronegativity of the O-containing substitute (phenolate) also enhances the intensity of the ν_{C-O}[47,48] and the $\delta_{ring\,C=C}$.[42] The spectrum of IM is also in agreement with these arguments. It is thus concluded that *m*-cresol adsorbs perpendicularly on the HT support surface probably through the methylene group mainly but it favours the adsorption through the OH group on the IM surface, orienting the ring parallel to the surface.

In the case of the HT support, after an hour exposure to steam (blue lines in Figure 9), the intensity of C—H stretching vibration of alkyl groups is lowered the most whereas other major vibration intensities of adsorbed species (e.g., $\nu_{C-H\,ring}$, ϕ, $\delta_{ring\,C=C}$, ν_{C-O}) decrease with similar relative ratios. This result suggests that under steam reforming conditions, some adsorbed methyl(ene) groups change, which can be oxidised, and the rest of these species (the ring and OH group) desorbs together. On the other hand, for IM support, during the steam reforming step, the intensity of C—O stretching vibration (1245 cm^{-1}) remain constant. Thus the anchoring point of *m*-cresol on IM support by the phenolate group is stable. In contrast, the C—H stretching for methyl(ene) vanishes and the intensity of ϕ decreases further than that of $\delta_{ring\,C=C}$. This phenomenon implies there is reaction occurring with the ring/methylene groups under the influence of steam. As the adsorbed species orients parallel to the surface, the reaction with steam can be more enhanced (more influence of the support) than that of the vertically adsorbed species on HT supports. Consequently, the amounts of species remaining on HT can be higher. This is in agreement with the TPO results for which more coke was found on used HT support than on IM support.

As Ni/HT exhibited the lowest amount of coke and worked better than Ni/IM, we only used Ni/HT for the IR investigation with supported Ni catalyst. In comparison with the spectra of the bare HT support (Figure 9B), the IR spectrum of Ni/HT (orange line in Figure 11) does not exhibit clear peaks for C—O stretching (ν_{CO}) vibration for carbonate or carboxylate in the region between 1600 and 1300 cm^{-1}.[42] Surprisingly, introduction of *m*-cresol did not lead to any sorption bands even after an hour exposure as observed for the HT support. This might indicate decomposition of *m*-cresol to IR-inactive species. To probe this further, the partial pressure of *m*-cresol in the vapour feed mixture was increased from 13 to 28 Pa for the adsorption of *m*-cresol on Ni/HT (corresponding to a *m*-cresol concentration of 128 ppm and 276 ppm, respectively). Howev-

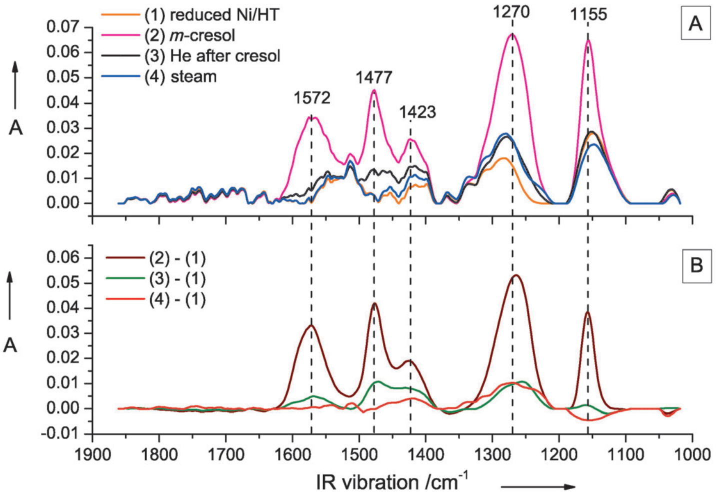

Figure 11. FTIR spectra recorded during titration-typed steam reforming of *m*-cresol on Ni/HT at 450 °C. A) Spectra after baseline correction; B) corresponding spectra after subtraction from the spectrum of the catalyst prior to the adsorption step.

er, even with the higher *m*-cresol concentration, it was hardly possible to observe any clear band for C–H stretching vibration of both aromatic (≈3050 cm^{-1}) or alkyl groups (2850–2925 cm^{-1}, not shown here). This lack of clear bands can be attributed to the activation of C–H cleavage by Ni. FTIR spectra in the low-wavenumber range recorded at the end of each step of the steam reforming on Ni/HT catalyst with higher *m*-cresol concentration are shown in Figure 11. In Figure 11 A the resulting spectra after baseline correction are shown and in Figure 11 B, the corresponding spectra subtracted from the spectrum of the catalyst prior to the adsorption step are shown, after the catalyst was reduced in H_2/He at 450 °C for an hour followed by evacuation in He for 30 min. Surprisingly, the peak positions in the range of 1700–1000 cm^{-1} of the adsorbed species on the catalyst are identical and similar to those of the species adsorbed on the bare IM support (Figure 9 A).

In the baseline-corrected spectra (Figure 11 A) the peak at 1423 cm^{-1} may be thought of as red-shifted CH_2 deformation,[42] but we did not observe any C–H stretching vibration. Thus, this is highly unlikely. As this region has features corresponding to those of COO^- ions,[42] it is possible that the missing methyl group from *m*-cresol is oxidised by ceria to form a carbonate or carboxyl group.

The absence of the OH band between 1320–1400 cm^{-1} and the enhanced intensity of the bands at 1477 and 1270 indicate the deprotonation in OH group of *m*-cresol. Thus this suggests that the adsorbed species anchor horizontally on the surface by both aromatic ring and phenolate groups. This is in agreement with the literature on adsorption of phenol on Ni surface as reported by Russell et al.[49] The difference spectra of (**3**, evacuation in He after *m*-cresol sorption) minus (**1**, clean reduced surface) as presented in Figure 11 B reveal the chemisorbed species on the catalyst. It can be seen that the ring C=C still remains on the surface. However, under the steam/He flow, the bands for the skeletal ring vibrations (1572 and 1477 cm^{-1}) are completely removed. No olefin intermediate (bands in the range of 1650–1800 cm^{-1}) is detected during all these experimental steps, suggesting that the 6C ring structure is disassociated at once on the Ni surface.

Among these three supported CeO_2–ZrO_2-based catalysts, Ni on Ce–Zr solid solution support synthesised by co-precipitation followed by hydrothermal treatment showed the best activity and stability in steam reforming of *m*-cresol (Figure 6 and 7). This catalyst has the highest content of Ce^{3+} in the bulk phase as well as on the catalyst surface (XPS and TPR data), which is proportional to the oxygen vacancy within the catalyst system in reductive atmosphere or oxygen mobility in oxidative reaction conditions. Mobile oxygen in the Ce–Zr solid solution can help in the oxidation of adsorbed molecules. The in situ FTIR study on reforming of *m*-cresol revealed that the sorption geometry/orientation of absorbed species are different in the two supported catalysts. In the case of Ni/HT, the methyl group may be oxidised by the interaction with the active site on the support in the vicinity of Ni active particles; the whole aromatic ring inclines to the metal surface on which deprotonation of the OH group takes place. Then the aromatic ring C interacts with Ni and is oxidised through steam-reforming reactions. The combination of the above-mentioned features leads to the excellent performance of Ni/HT catalyst. The catalysis of steam *m*-cresol reforming seems to involve manifold sites including Ce and Ni with multiple Ni sites, which implies that larger Ni crystallites may be favoured and there should be an optimum as ceria is also involved.

Conclusions

For the steam reforming of *m*-cresol, Ni supported on CeO_2–ZrO_2 prepared by co-precipitation followed by hydrothermal treatment (Ni/HT) was the most promising of three CeO_2–ZrO_2-supported Ni catalysts. The hydrothermal treatment, besides improving the thermal resistance of the support, provides high concentration of Ce^{3+} on the surface as well as the bulk phase of the solid solution. This in turn improves the redox nature of the catalysts, which contributes to its tremendous capability in steam reforming and coke oxidation through redox reactions. The supported Ni attributes to the major activity in breaking the C–C and C–H bonds of *m*-cresol. An in situ FTIR study revealed the horizontal adsorption of the aromatic rings on the Ni surface and interaction of the methyl group with the support. This orientation allows multiple cleavages to occur concomitantly on the catalyst.

Experimental Section

Syntheses of Ce–Zr mixture

Mixed Ce–Zr oxide was prepared by the co-precipitation method. Stoichiometric amounts of $Ce(NO_3)_3{\cdot}6H_2O$ and $ZrO(NO_3)_2{\cdot}6H_2O$ (Ce/Zr 0.25) were dissolved in demineralised water. The initial pH of this solution was approximately 0.5. The solution was heated to 80 °C under vigorous magnetic agitation. A 10% solution of NH_3 was slowly added drop-wise into the precursor solution until the pH reached 8.5 to precipitate most of the precursor species (the gel of cerium–zirconium hydroxide complex started forming at pH ≈3.5). The cerium–zirconium gel was then filtered with a Büchner funnel and washed with demineralised water until the effluent reached neutral pH. A part of the gel was then dried at 80 °C in a vacuum dryer overnight prior to calcination in air (see below). This solid powder after calcination was denoted as CP as it was made through the co-precipitation method. Other part of the gel after the co-precipitation step was transferred to a 100 mL non-stirred autoclave with Teflon liner. A 40 mL volume of 40 wt.% KOH was added to the gel. The sealed autoclave was then heated to 180 °C and maintained at this temperature for 24 h in a static oven. Afterward, the autoclave was slowly cooled down to RT. The product was then filtered and washed with a large amount of demineralised water until the pH of the effluent became neutral (pH ≈ 8). The sample was subsequently dried in a vacuum oven overnight followed by calcination in air. The final product obtained after the calcination step was denoted HT (hydrothermal treatment).

Commercial monoclinic ZrO_2 oxide (RC-100, Gimex Technisch Keramik B.V.) was first calcined in air at 800 °C with a flow rate of 50 $cm^3\,min^{-1}$ for 6 h (heating or cooling rate 5 °C min^{-1}). Ceria was deposited onto *m*-ZrO_2 through the wet impregnation method. $Ce(NO_3)_3{\cdot}6H_2O$ was dissolved in 50 mL demi-water. *m*-ZrO_2 was then dispersed in the $Ce(NO_3)_3$ solution. The solvent was then removed by using a rotary evaporator under vacuum. Subsequently, the sample was dried further in a vacuum oven at 80 °C overnight. After subjecting to calcination treatment, the support prepared by the impregnation route was denoted as IM (impregnation).

Solid samples obtained after drying in the vacuum oven, were then heated in air with a flow rate of 50 $cm^3 min^{-1}$. The furnace was first heated to 150 °C with a temperature ramp of 5 °C min^{-1} and kept at 150 °C for 1 h. Then, the furnace temperature was increased to 725 °C with a heating rate of 5 °C min^{-1}, kept at that temperature for 6 h prior to cooling down to RT at a rate of 5 °C min^{-1}.

Deposition of nickel

Nickel was deposited on these supports by the homogeneous deposition–precipitation technique. Typically, $Ni(NO_3)_3 \cdot 6H_2O$ (99 %, 0.1734 g) was dissolved in demineralised water in a round flask with vigorous agitation. Then the support (≈1 g) was dispersed in the solution. The mixture was preheated to 75 °C. A solution containing approximately 4.5 g urea was poured into the mixture at this point. The total volume of liquid was 250 mL. Subsequently, the temperature was increased to 90 °C and the mixture was kept at this temperature until the deposition was completed (4–5 h, final pH of 7.5). Samples were then filtered and washed with demineralised water prior to drying in the vacuum oven (80 °C) for 3 h. After that, the solid samples were calcined (air flow rate 50 $cm^3 min^{-1}$) at 500 °C for 3 h with a heating rate of 5 °C min^{-1}. All catalysts were reduced in 10 vol.% H_2/N_2 at 650 °C (ramping temperature 10 °C min^{-1}) for 3 h. After the reduction step, catalysts were denoted as Ni/CP, Ni/HT, Ni/IM, respectively.

Catalyst characterisation

The textures of these catalysts (specific area, pore size distribution) were determined from liquid nitrogen adsorption/desorption isothermal curves acquired with a Micromeritics TriStar instrument. Samples were degassed at 300 °C prior to the analysis. X-ray diffraction data were recorded with a Bruker D2 Phaser diffractometer using $Cu_{K\alpha}$ radiation, $\lambda = 0.1544$ nm. Elemental compositions of the catalysts were analysed by an X-ray fluorescence spectrometer (Philips PW 1480). XPS analysis was performed with a Quantera SXM (scanning XPS microprobe) spectrometer from Physical Electronics. X-ray (Al K_α) power of 50 W, 20 mA and a beam size 200 μm were used.

TPR or TPO was performed in a homebuilt set-up. For TPO and TPR measurement, the catalysts or supports (10–50 mg), respectively, with grain sizes of 0.3–0.6 mm were packed between two quartz plugs in a 4 mm (i.d.) α-alumina tube. Before TPR or TPO analysis, samples were pre-treated in Ar at 150 °C for 30 min. Then the oven was cooled to RT. For TPR analysis, a 5 vol.% H_2/Ar mixture with a flow rate of 25 $cm^3 min^{-1}$ was used. H_2 consumption was monitored with a standard thermal conductivity detector calibrated by H_2 reduction of NiO (purity 99.999 %). For TPO analysis, a 1 vol.% O_2/He mixture with a flow rate of 75 $cm^3 min^{-1}$ was sent through the reactor. The gas outlet containing CO or CO_2 was sent (split ratio 6 %) to an online methanizer (Model 110 Chassis, SRI Instruments Europe GmbH) equipped with a flame ionisation detector (FID). The CO_x produced was calibrated by using $Al_2(CO_3)_3$ as a carbon source standard (the C content of $Al_2(CO_3)_3$ was determined by a CHNS elemental analyser mentioned elsewhere[8]). In a typical TPR or TPO measurement, the furnace was heated to 700 °C with heating ramp of 5 °C min^{-1}, then kept at that end temperature for 30 min before cooling down to RT (10 °C min^{-1}).

Raman spectroscopy data were obtained with a Bruker Senterra Raman spectrometer (laser wavenumber 532 cm^{-1}) at ambient conditions. The spectra were recorded with a laser power of 5 mW, exposition time of 1–2 s. The spectra represent 50–100 scans with a spectral resolution of 3–5 cm^{-1}.

Catalytic testing

The catalysts or supports (15 mg) with a grain size of 0.3–0.6 mm were packed in an α-alumina fixed-bed reactor (i.d. 4 mm) and held in place between two quartz wool plugs. The catalyst/support was first reduced in situ in 10 vol.% H_2/Ar (flow rate 50 $cm^3 min^{-1}$, temperature ramp 10 °C min^{-1}) at 650 °C for 1 h. The reactor was then purged with Ar for approximately 30 min before the furnace temperature was raised to 700 °C. An aqueous solution of *m*-cresol (≈20 g L^{-1}) was sent to an evaporator by using a syringe pump (ISCO Model 500 D). The solution was vaporised at 140 °C. The *m*-cresol/steam mixture was carried to the reactor by an Ar flow (flow rate 25 $cm^3 min^{-1}$). Ar was also used as an internal standard gas for the outlet gas mixture. With such flow rates, the weight hourly space velocity (WHSV) of *m*-cresol equalled 7.89 h^{-1}. The outlet gas stream passed a flash separator in which the condensed liquid was sampled every hour and the gas was sent directly to an online Varian gas chromatograph (GC, CP-3800) with three parallel separation channels using multiple GC columns (channel 1: Hayesep Q, Hayesep T, Molsieve 13X; channel 2: Hayesep Q, Molsieve 5A; channel 3: CP Wax 52CB). The GC was equipped with thermal conductivity detectors for quantification of permanent gases (CO, CO_2, H_2 and Ar) and a FID for quantification of hydrocarbons.

Condensed liquid from the flash separator was analysed offline with a Shimadzu reverse phased High Performance Liquid Chromatograph Prominence system equipped with a Hypesil Gold column and a UV detector ($\lambda = 254$ nm). A mobile phase containing water/methanol 40:60 (v/v) with a flow rate of 0.5 mL min^{-1} was used for analysis. The column oven was kept at 40 °C. Typically, it took 15 min to perform an analysis.

m-Cresol conversion was calculated as the mole of *m*-cresol reacted divided by the moles of *m*-cresol in the feed. The amounts of unconverted *m*-cresol were calculated from HPLC data with the assumption that the amount of *m*-cresol in the gas stream to GC was negligible. Thus the condensed liquid volume was theoretically estimated, based on the feed concentration and water consumed in Reactions (1) and (2). Hydrogen yield was defined as the mole of hydrogen produced divided by the maximum amount of H_2 that can be produced based on Reaction (1):

$$C_7H_8O + 13\,H_2O \rightarrow 7\,CO_2 + 17\,H_2 \tag{1}$$

$$C_7H_8O + 6\,H_2O \rightarrow 7\,CO + 10\,H_2 \tag{2}$$

Therefore, yields of and selectivities to H_2, CO_x and phenol were calculated as shown in Equations (3)–(7):

$$\text{Yield of } H_2\ (\%) = \frac{\text{mole of hydrogen produced}}{17 \times \text{mole of } m\text{-cresol feed}} \times 100 \tag{3}$$

$$\text{Yield of phenol}\ (\%) = \frac{6 \times \text{mole of phenol}}{7 \times \text{mole of } m\text{-cresol feed}} \times 100 \tag{4}$$

$$\text{Yield of } CO_x\ (\%) = \frac{\text{mole of } CO_x}{7 \times \text{mole of } m\text{-cresol feed}} \times 100 \tag{5}$$

$$\text{Selectivity to phenol } (\%) = \frac{6 \times \text{mole of phenol}}{7 \times \text{mole of } m\text{-cresol reacted}} \times 100 \tag{6}$$

$$\text{Selectivity to CO}_x\ (\%) = \frac{\text{mole of CO}_x}{7 \times \text{mole of } m\text{-cresol reacted}} \times 100 \tag{7}$$

In situ FTIR study on reforming of *m*-cresol

Transmission FTIR spectra were recorded by using a Bruker Vector 22 equipped with an MCT detector with a time interval of 120 s. Each spectrum was the average of 128 scans with a spectral resolution of 4 cm^{-1}. Typically, a self-supporting disc (sample amount ≈10 mg) was placed into a purpose-built stainless-steel cell. FTIR spectra of the empty cell with helium flow (20 $cm^3 min^{-1}$) at 21 °C were recorded and used as background. *m*-Cresol reforming reactions were performed on a titration basis. Samples were pre-treated in 10 vol.% H_2/He (flow rate 20 $cm^3 min^{-1}$, temperature ramp 10 °C min^{-1}) at 450 °C for an hour. The IR cell containing samples was then outgassed with He for 30 min prior to adsorption of *m*-cresol and then steam. Each adsorption step was performed for an hour and followed by flushing the cell with He for 30 min. For the *m*-cresol adsorption or steam adsorption, He was flown through a saturator at 21 °C filled with *m*-cresol (Sigma Aldrich >98% purity) or filled with demineralised water, respectively, resulting in a *m*-cresol partial pressure of 13 Pa (estimated from Antoine equation formula proposed by Biddiscombe and Martin[50]) or a H_2O partial pressure of approximately 2500 Pa, respectively. The tubing from saturators to the cell was heated at 150 °C to prevent condensation.

Acknowledgements

This research has been performed within the framework of the CatchBio program. The authors gratefully acknowledge the support of the Smart Mix Program of the Netherlands Ministry of Economic Affairs, Agriculture and Innovation and the Netherlands Ministry of Education, Culture and Science. Project number 053.70.113. The authors acknowledge Bert Geerdink for development of TPR/TPO analysis, Louise Vrielink and Tom Velthuizen for XRF analysis, Karin Altena-Schildkamp for BET analysis, Dr. Songbo He for assisting in catalytic tests. The authors are also grateful to Dr. Arie van Houselt and Dr. Shilpa Agarwal for helpful discussions about FTIR.

Keywords: oxidation · hydrogen · nickel · arenes · cerium

[1] G. W. Huber, S. Iborra, A. Corma, *Chem. Rev.* **2006**, *106*, 4044–4098.

[2] D. M. Alonso, J. Q. Bond, J. A. Dumesic, *Green Chem.* **2010**, *12*, 1493–1513.

[3] E. Kırtay, *Energy Convers. Manage.* **2011**, *52*, 1778–1789.

[4] R. M. Navarro, M. C. Sanchez-Sanchez, M. C. Alvarez-Galvan, F. del Valle, J. L. G. Fierro, *Energy Environ. Sci.* **2009**, *2*, 35–54.

[5] R. M. Navarro, M. A. Pena, J. L. Fierro, *Chem. Rev.* **2007**, *107*, 3952–3991.

[6] D. Dayton in *Milestone Completion Report*, National Renewable Energy Laboratory, **2002**.

[7] M. M. Yung, W. S. Jablonski, K. A. Magrini-Bair, *Energy Fuels* **2009**, *23*, 1874–1887.

[8] T. M. C. Hoang, L. Lefferts, K. Seshan, *ChemSusChem* **2013**, *6*, 1651–1658.

[9] C. Wu, R. H. Liu, *Int. J. Hydrogen Energy* **2010**, *35*, 7386–7398.

[10] C. Wu, R. Liu, *Energy Fuels* **2010**, *24*, 5139–5147.

[11] A. Ishihara, E. W. Qian, I. N. Finahari, I. P. Sutrisna, T. Kabe, *Fuel* **2005**, *84*, 1462–1468.

[12] M. Marquevich, S. Czernik, E. Chornet, D. Montané, *Energy Fuels* **1999**, *13*, 1160–1166.

[13] J. Han, H. Kim, *Renewable Sustainable Energy Rev.* **2008**, *12*, 397–416.

[14] T. Kimura, T. Miyazawa, J. Nishikawa, S. Kado, K. Okumura, T. Miyao, S. Naito, K. Kunimori, K. Tomishige, *Appl Catal B* **2006**, *68*, 160–170.

[15] R. Di Monte, J. Kašpar, *J. Mater. Chem.* **2005**, *15*, 633.

[16] P. Fornasiero, R. Dimonte, G. R. Rao, J. Kaspar, S. Meriani, A. Trovarelli, M. Graziani, *J. Catal.* **1995**, *151*, 168–177.

[17] G. Colón, M. Pijolat, F. Valdivieso, H. Vidal, J. Kašpar, E. Finocchio, M. Daturi, C. Binet, J. C. Lavalley, R. T. Baker, S. Bernal, *J. Chem. Soc. Faraday Trans.* **1998**, *94*, 3717–3726.

[18] G. Vlaic, R. Di Monte, P. Fornasiero, E. Fonda, J. Kašpar, M. Graziani, *J. Catal.* **1999**, *182*, 378–389.

[19] B. Matas Güell, I. V. Babich, L. Lefferts, K. Seshan, *Appl. Catal. B* **2011**, *106*, 280–286.

[20] Y.-Q. Song, H.-M. Liu, D.-H. He, *Energy Fuels* **2010**, *24*, 2817–2824.

[21] B. K. Kim, H. O. Hamaguchi, *Phys. Status Solidi B* **1997**, *203*, 557–563.

[22] E. Anastassakis, B. Papanicolaou, I. M. Asher, *J. Phys. Chem. Solids* **1975**, *36*, 667–676.

[23] T. Hirata, E. Asari, M. Kitajima, *J. Solid State Chem.* **1994**, *110*, 201–207.

[24] T. Hirata, *J. Phys. Chem. Solids* **1995**, *56*, 951–957.

[25] D. J. Kim, J. W. Jang, H. L. Lee, *J. Am. Ceram. Soc.* **1997**, *80*, 1453–1461.

[26] P. Biswas, D. Kunzru, *Int. J. Hydrogen Energy* **2007**, *32*, 969–980.

[27] R. Hu, C. Yan, X. Zheng, H. Liu, Z.-y. Zhou, *Int. J. Hydrogen Energy* **2013**, *38*, 6033–6038.

[28] R. Si, Y.-W. Zhang, S.-J. Li, B.-X. Lin, C.-H. Yan, *J. Phys. Chem. B* **2004**, *108*, 12481–12488.

[29] C. Diagne, H. Idriss, A. Kiennemann, *Catal. Commun.* **2002**, *3*, 565–571.

[30] J. Fan, X. Wu, R. Ran, D. Weng, *Appl. Surf. Sci.* **2005**, *245*, 162–171.

[31] A. Laachir, V. Perrichon, A. Badri, J. Lamotte, E. Catherine, J. C. Lavalley, J. El Fallah, L. Hilaire, F. Le Normand, E. Quéméré, G. N. Sauvion, O. Touret, *J. Chem. Soc. Faraday Trans.* **1991**, *87*, 1601.

[32] A. Pfau, K. D. Schierbaum, *Surf. Sci.* **1994**, *321*, 71–80.

[33] S. Watanabe, X. L. Ma, C. S. Song, *J. Phys. Chem. C* **2009**, *113*, 14249–14257.

[34] H. Vidal, J. Kašpar, M. Pijolat, G. Colon, S. Bernal, A. Cordón, V. Perrichon, F. Fally, *Appl. Catal. B* **2001**, *30*, 75–85.

[35] H. Vidal, J. Kašpar, M. Pijolat, G. Colon, S. Bernal, A. Cordón, V. Perrichon, F. Fally, *Appl. Catal. B* **2000**, *27*, 49–63.

[36] J. Nishikawa, K. Nakamura, M. Asadullah, T. Miyazawa, K. Kunimori, K. Tomishige, *Catal. Today* **2008**, *131*, 146–155.

[37] N. Hickey, P. Fornasiero, J. Kašpar, J. M. Gatica, S. Bernal, *J. Catal.* **2001**, *200*, 181–193.

[38] S. Salasc, V. Perrichon, M. Primet, M. Chevrier, N. Mouaddib-Moral, *J. Catal.* **2000**, *189*, 401–409.

[39] X. J. Li, J. Hayashi, C. Z. Li, *Fuel* **2006**, *85*, 1700–1707.

[40] A. C. Ferrari, J. Robertson, *Phys. Rev. B* **2000**, *61*, 14095–14107.

[41] J. Schwan, S. Ulrich, V. Batori, H. Ehrhardt, S. R. P. Silva, *J. Appl. Phys.* **1996**, *80*, 440–447.

[42] N. B. Colthup, L. H. Daly, S. E. Wiberley, *Introduction to infrared and Raman spectroscopy*, Academic Press, United State of America, **1990**.

[43] S. Benfer, E. Knozinger, *J. Mater. Chem.* **1999**, *9*, 1203–1209.

[44] G. Cerrato, S. Bordiga, S. Barbera, C. Morterra, *Appl. Surf. Sci.* **1997**, *115*, 53–65.

[45] J. Kondo, H. Abe, Y. Sakata, K.-i. Maruya, K. Domen, T. Onishi, *J. Chem. Soc. Faraday Trans. 1* **1988**, *84*, 511–519.

[46] C. Binet, M. Daturi, J. C. Lavalley, *Catal. Today* **1999**, *50*, 207–225.

[47] H. Miyata, T. Ohno, F. Hatayama, *J. Chem. Soc. Faraday Trans.* **1995**, *91*, 3505–3510.

[48] L. Palmisano, M. Schiavello, A. Sclafani, G. Martra, E. Borello, S. Coluccia, *Appl. Catal. B* **1994**, *3*, 117–132.

[49] J. N. Russell, S. S. Sarvis, R. E. Morris, *Surf. Sci.* **1995**, *338*, 189–203.

[50] D. P. Biddiscombe, J. F. Martin, *Trans. Faraday Soc.* **1958**, *54*, 1316–1322.

Received: October 23, 2014